Nuclear Inst. and Methods in Physics Research, A 1053 (2023) 168382

Contents lists available at ScienceDirect

Nuclear Inst. and Methods in Physics Research, A

journal homepage: www.elsevier.com/locate/nima

Full Length Article

A calibration system for hadron synchrotrons with a large frequency swing

Aleksandr Andreev [a], Dieter Lens [a,*], Harald Klingbeil [a,b]

[a] GSI Helmholtzzentrum für Schwerionenforschung GmbH, Planckstraße 1, Darmstadt, 64291, Germany
[b] Technische Universität Darmstadt, Schloßgartenstraße 8, Darmstadt, 64289, Germany

ARTICLE INFO

Keywords:
Direct digital synthesis (DDS)
Phase measurement
Heavy ion synchrotron
Time-domain analysis

ABSTRACT

The synchronization of radio frequency (RF) systems in hadron synchrotrons relies on the availability of reference RF signals with a precise phase. For accelerators with a large frequency swing, frequency dependent phase errors can exceed the required phase margin and therefore have to be compensated. In this paper a new method for the phase calibration of RF signals with variable frequency is described. All the signals are measured with a digital oscilloscope and no complex signal processing is necessary. The described approach utilizes a three-parameter sine wave fit algorithm to estimate the phase of the relevant sine wave signals. A phase difference between RF signals with different frequencies is then calculated with respect to a reference pulse train. A detailed analysis of the measurement parameters is given. The method is applied for the calibration of the RF reference signals of the heavy ion synchrotron SIS18 at GSI.

1. Introduction

One of the main features of heavy ion synchrotrons, allowing to accelerate ions of different species up to relativistic energies, is a large frequency swing [1,2]. Depending on the machine's circumference and the harmonic numbers, their typical frequency span is usually within the range from a few kHz to tens of MHz [3].

The Facility for Antiproton and Ion Research (FAIR) is an accelerator complex under construction in Darmstadt [4,5]. It incorporates the existing facilities of GSI and also several new accelerators, which are being built within the project. The largest of them, SIS100 [6], is a new heavy ion synchrotron utilizing RF cavities to perform longitudinal ion beam manipulations. Besides the realization of several new RF systems for SIS100 and the storage rings CR and HESR, the FAIR project also includes an upgrade of the RF systems of the existing accelerator rings such as the heavy ion synchrotron SIS18 and the experimental storage ring ESR. One of the key parameters of the FAIR research program is a high beam intensity, i.e. a large beam current. In order to increase the average beam intensity, the synchrotron has to provide ion beams with a high repetition rate, i.e. short cycle times with fast ramping [7].

In order to increase the precision of the accelerating sinusoidal radio frequency (RF) voltage acting on the charged particles, Direct Digital Synthesis (DDS) generators are widespread in modern synchrotrons to generate reference signals, which are then used to drive the accelerating cavities and other RF systems of the accelerator. They allow to implement digital systems (except for the output stage, where the analog voltage is produced), which, among other advantages, provide the possibility to implement automated calibration procedures [8]. Phase measurement systems described in the literature [9–13] allow to achieve phase measurement accuracies better than hundredths of a degree, and thus are of interest for current and upcoming generations of accelerators.

The Low-Level Radio Frequency (LLRF) architecture for FAIR depends on so-called Group DDS signals as the fundamental reference signals for the cavity synchronization [14]. In order to reach the desired beam quality, this synchronization must realize a phase accuracy of better than ±3° under dynamic conditions (i.e. during acceleration). For every supply area of a FAIR synchrotron, the Group DDS system consists of several modules, where each module can be configured with a separate harmonic number. As the analog output signal of every Group DDS module is part of the cavity synchronization (for a group of RF cavities with the same harmonic number), its phase accuracy must be much better than ±3°. Typically, a phase accuracy of better than ±1° under dynamic conditions is required.

To reach this accuracy, a calibration is needed to compensate frequency-dependent phase inaccuracies in the analog output stage of each Group DDS module. This calibration must cover RF frequencies between 215 kHz and 5.4 MHz and ramp rates of up to 10 MHz/s. For larger flexibility during beam operation of the FAIR synchrotrons with respect to multi-harmonic operation, it shall be possible in future to change harmonic numbers of the Group DDS modules during beam operation. Therefore, the calibration result must be valid for arbitrary configurations of harmonic numbers.

This paper presents a new phase calibration technique designed to meet these requirements. It is a significantly extended version of [15]

* Corresponding author.
E-mail address: d.e.m.lens@gsi.de (D. Lens).

https://doi.org/10.1016/j.nima.2023.168382
Received 8 March 2023; Received in revised form 2 May 2023; Accepted 15 May 2023
Available online 18 May 2023

and presents a method for the phase calibration of sinusoidal RF signals with variable frequencies using sine wave fit algorithms. After development and optimization in a laboratory setup, the calibration has been successfully deployed and tested with multi-harmonic beam operation in SIS18, where it is now used in standard operation. Since the implementation of the proposed method in each particular case is related to addressing the challenges associated with the specific features of each RF system, we describe all aspects in detail, referring to our application. However, the method is applicable to all systems utilizing a digital frequency synthesizer with an analog output, where information on the precise activation of digital data is available.

The paper is structured as follows. First, Section 2 introduces the Group DDS concept as part of the LLRF architecture for the ring accelerators and storage rings of FAIR. Next, a brief overview of phase measurement techniques is given in Section 3, followed by the formulation of the multi-harmonic phase calibration problem. Section 4 gives a detailed description of the realized method and summarizes the calibration procedure. A recommended choice of the measurement parameters is discussed in Section 5. An application example with the measurement results is presented in Section 6, and Section 7 discusses further steps that are needed for multi-harmonic operation. Finally, Section 8 concludes and presents an outlook.

2. Group DDS concept and calibration

2.1. LLRF topology

Typically, the Group DDS in an RF supply area consists of four modules that are denoted by the letters A to D mounted together in one Group DDS module crate, cf. Fig. 1. Each of the DDS modules receives the revolution frequency ramp f as well as a harmonic number h from the Central Control System (CCS), which allows them to generate multiples of the fundamental frequency and thus perform multi-harmonic operations. The ramp data is distributed via the Scalable Control Unit (SCU, cf. [16]) frontend hardware. In addition, each module receives two clocks of the Bunch Phase Timing System (BuTiS) and dedicated White Rabbit (WR) Timing events, such as the phase reset event and the event for the start of the function generators. The output of each Group DDS module is a sinusoidal reference signal with an RF frequency of $h \cdot f$.

As shown in Fig. 1, the principle of the cavity synchronization is based on the distribution of reference and gap signals via a Switch Matrix to the cavity synchronization subsystems. This enables to have synchronized RF signals at any location of the facility [14]. For each cavity system, two signals (reference and gap) are distributed on equivalent signal transmission paths to the cavity synchronization subsystems, such that the phase between both signals can be measured as part of the cavity synchronization feedback loop. By equivalent we understand signal paths that contain the same type of electronic modules, transmission lines etc., such that the frequency-dependent phase response of the complete signal transmission chain is comparable for both signals (within the required phase accuracy, i.e. better than $\pm 1°$). For a specific cavity system, the reference signal and the gap signal are assumed to have the same RF frequency. This is established by the Switch Matrix, which is configured such that each cavity system receives a reference signal from a Group DDS module with the harmonic number at which the cavity system is operated. Since the gap signals are required for multiple purposes (further feedback loops, diagnosis systems, etc.), distribution amplifier (DA) modules that duplicate RF signals are needed in the signal transmission paths.

A Group DDS oscilloscope is used to monitor the analog output signals of the Group DDS modules. Any phase deviation or imperfection in the signal chain before this oscilloscope has to be corrected by the Group DDS calibration that is described in the following. These imperfections can e.g. result from the output stages of the DDS modules, signal lines, and electronic modules such as the DA. The calibrated signals at the Group DDS oscilloscope and the gap voltages in the accelerator tunnel have by definition the delay value $\tau = 0\,\mathrm{s}$. These delay levels are marked as gray boxes in Fig. 1.

The RF cavities of the SIS100 synchrotron are distributed along the 6 sectors of the ring with a circumference of about $1084\,\mathrm{m}$ and several RF supply areas exist at different locations. Due to the fast ramp rates with a large frequency swing distributing the analog sinusoidal RF signals from one main central oscillator would be technically extremely difficult. Thus, unlike in other designs [17–21], instead of using one central reference the reference RF signals for FAIR are generated locally in more than 8 RF supply areas by different Group DDS modules.

In every RF supply area of the FAIR campus, the Group DDS modules must therefore produce phase-synchronous signals. The time synchronization of these signals is ensured with a precision timing and clock distribution system called BuTiS (cf. [22]), and all DDS modules are fed with the same ramp data (revolution frequency and harmonic number) provided by the CCS.

In order to synchronize the DDS units they are fed with two phase-synchronous delay-compensated external clock signals with the frequencies 25 MHz and 100 kHz (referred to as T_0) from the BuTiS clock distributor amplifier [22]. The 25 MHz signal is used as a general DDS clock signal. It ensures that the RF signals generated by different DDS modules will not deviate over time. The T_0 identifier pulse train enables synchronized command execution (such as the start of a frequency ramp) at different locations of the facility. This principle, called resynchronization, is the basis for phase-synchronous frequency-variable RF signals at different locations of the facility [23] and is illustrated in Fig. 2. Commands are distributed between two rising slopes of the first clock signal T_0 to all DDS modules. For example, the purpose of such a command may be starting a frequency ramp or resetting the phase accumulator. Different channels for command distribution exist, such as the SCU backplane or telegrams via optical fibers. The commands are usually activated at dedicated WR events. Since BuTiS and WR are synchronized, it is guaranteed that the commands are distributed between two rising T_0 slopes. The 25 MHz clock signal has an accuracy that is typically better than $100\,\mathrm{ps}$ and enables the required accuracy of the DDS. It is aligned such that its falling slopes coincide with the rising T_0 slopes. With this setup, available commands are executed at the first (or in general, at the n^{th}) rising slope of the 25 MHz clock after the next (or in general, also at any pre-defined subsequent) rising T_0 slope, cf. Fig. 2.

2.2. Group DDS calibration

Although the DDS allows to maintain the phase stability of the generated RF signals, the output stage where the digital signal is transformed into an analog sinusoidal voltage may introduce undesired phase deviations. Without countermeasures, different operating frequencies of the DDS modules in combination with manufacturing tolerances and environmental influences would lead to undesired phase shifts between the reference RF signals due to a frequency-dependent phase response of DDS modules. Additional cables and modules before the Group DDS oscilloscope are a further source of such phase errors.

For this reason the topology of the supply area includes Calibration Electronic Modules (CEL, [24,25]), each of which compensates for the phase response of the dedicated DDS module. As shown in Fig. 3, during the standard operation each CEL module receives telegrams with the DDS RF frequency $h \cdot f$ via optical fiber link and provides optical telegrams with phase corrections $\phi_{\mathrm{corr},hf}$ to the DDS module it is correcting.

Another important requirement is a long term stability of the calibration. Frequent recalibrations will increase the time required for the accelerator maintenance. Once the system is calibrated, it is planned to repeat the calibration once per season (e.g. summer and winter) for monitoring purposes. It also should be repeated if any of the compo-

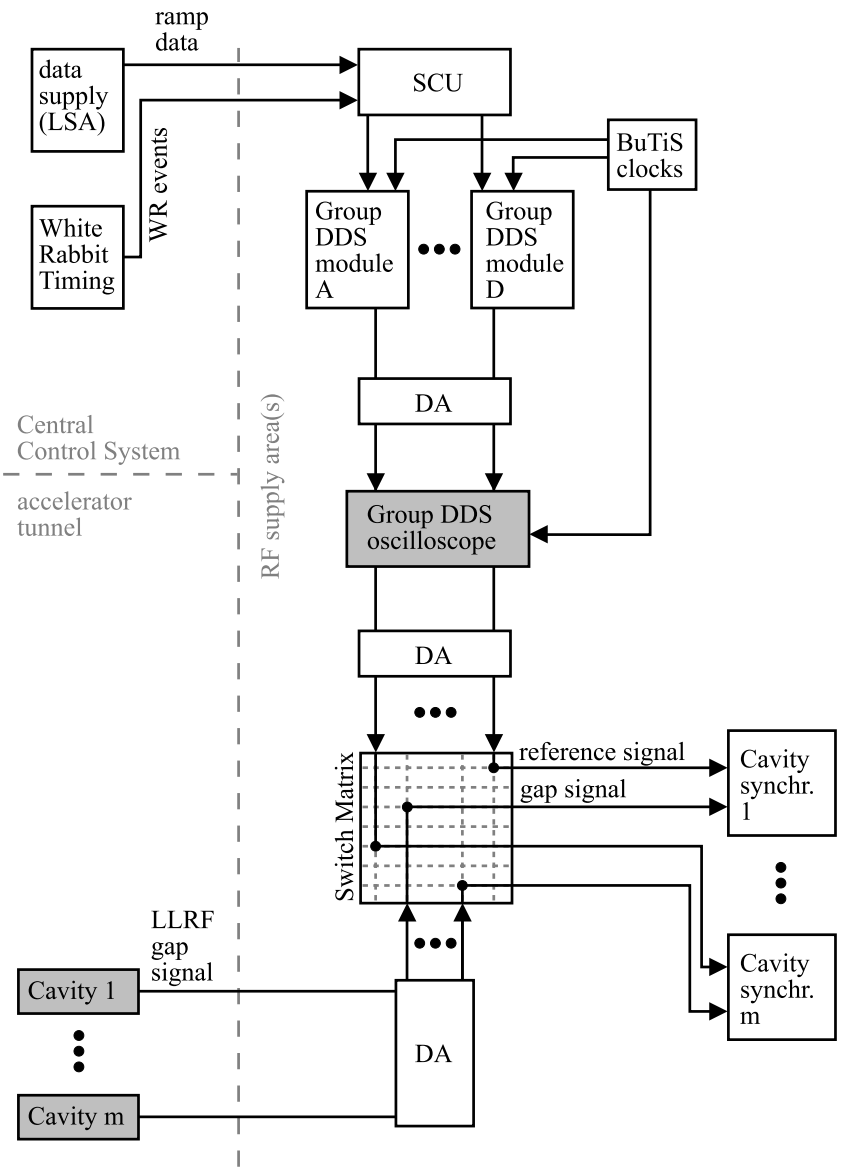

Fig. 1. Concept of signal distribution for the cavity synchronization.

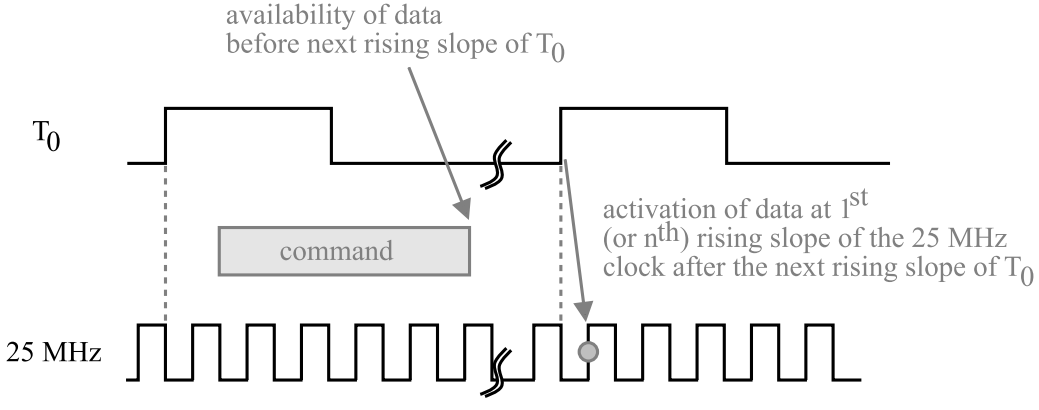

Fig. 2. BuTiS clock signals and resynchronization.

nents of the LLRF system is replaced. In any case, the time needed for the calibration of one frequency synthesizer should be minimized. Until now, we have not observed significant changes over the year as long as the LLRF setup (hardware, firmware, cables, etc.) is not changed. Phase drifts due to temperature changes or aging effects will be studied during the next years.

The calibration described in this paper is performed during maintenance periods of the synchrotron. This makes it possible for the

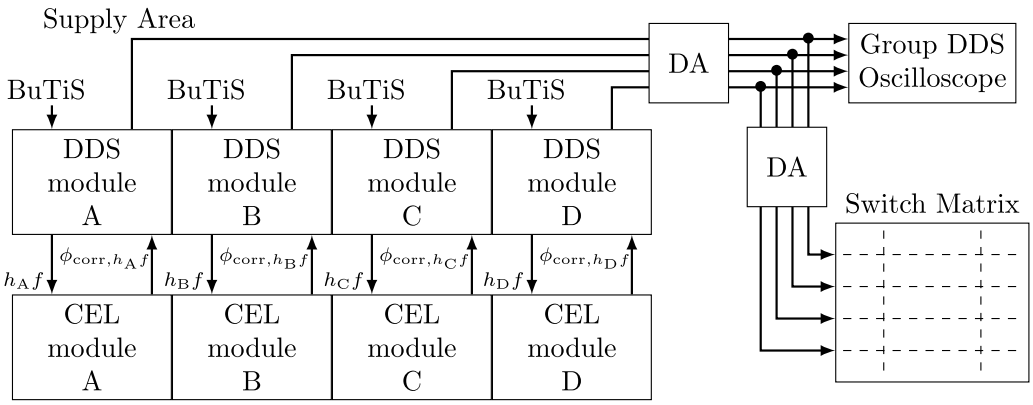

Fig. 3. Topology of the Group DDS calibration.

calibration algorithm to fully control the front end hardware (SCU) that hosts the Group DDS modules which would not be possible during beam operation. During calibration, stationary sine waves with constant frequencies are used.

3. Multi-harmonic phase calibration

3.1. State-of-the-art measurement techniques

The task to measure an RF signal's phase can be solved by numerous techniques [26,27]. A zero crossing detection, virtual vector-voltmeter, discrete Fourier transform (DFT) or interpolated discrete Fourier transform (IpDFT) and estimation by sine wave least squares fit can be applied depending on the required accuracy level and signal's characteristics. Applying sine fitting algorithms, as recommended by the standards [28,29], allows avoiding the necessity to ensure a coherent sampling of the RF signal at different frequencies, which simplifies the implementation of the measurement method. The fitting may either include an estimation of the frequency ("unknown frequency model"), or the frequency is determined independently ("known frequency model"). A criterion for selecting the known or unknown frequency model is derived in [30].

A well-known approach is to determine the frequency separately and apply a *three parameter sine fit (3PSF)* instead of computing the direct *four parameter sine fit (4PSF)* in order to reduce the computational complexity [31–35]. Both fit algorithms are discussed in more detail in Section 4.2. For frequency estimation one can use a one dimensional grid search [30,32], IpDFT [33,34,36] or iterative IpDFT [37] methods. In [38] it was demonstrated that a comparable accuracy can be achieved by both algorithms if enough data samples are used. Improved sine fit algorithms for sequential sampling were proposed recently [39].

The 3PSF and 4PSF algorithms were selected in favor of other methods due to their high accuracy, robustness in case of noncoherent sampling, and simplicity in terms of implementation [27,40–42]. For the 3PSF algorithm it is assumed that the frequency is *a priori* known (which is the case during calibration conditions with constant frequencies), and the actual frequency of the generator derived from the frequency tuning word (FTW) is used. A one-dimensional grid search is employed to obtain the estimate for the frequency when the unknown frequency model is applied [32].

3.2. Absolute phase calibration

Different, variable harmonic numbers of the DDS modules lead to a number of possible combinations for measuring relative phases between the modules with a certain frequency ratio. In order to reduce the number of possible combinations, an absolute phase calibration of Group DDS modules in different supply areas was implemented [15], where each DDS module operates at fundamental harmonic, i.e. $h = 1$, and their common clock signal is used as a reference for the calibration. The frequency range under calibration is determined by the highest desired harmonic number h_{max} and the highest fundamental frequency f_{max} and, therefore, covers the DDS RF frequencies from the lowest fundamental frequency f_{min} to $h_{\mathrm{max}} \cdot f_{\mathrm{max}}$. When operating at the harmonic number h, the DDS module produces a sine wave with the frequency $h \cdot f$ and sends it to the CEL module, which tracks changes of the DDS RF frequency. The corresponding phase correction value for this frequency applied by the CEL module leads to a corrected analog DDS output with the right phase. This approach requires no additional assumptions and thus, allows for using the same calibration data independent of the harmonic number of each DDS module in later operation. Due to this procedure, the phase correction only depends on the product $h \cdot f$ and not on the specific choice of h or f.

4. Proposed measurement method

4.1. Resynchronization and trigger sequence

The synchronization of the frequency ramp with the timing events is performed by the field programmable gate array (FPGA) of the DDS module (Fig. 4). As a first step an FTW is preloaded into the DDS by the SCU and synchronized with the next timing event (Start-Tag). After decoding and internal processing of the Start-Tag event the DDS performs a phase reset of the phase accumulator and switches a signal on a trigger output to logical "high" state, which is used as an identifier pulse for the calibration procedure. The DDS then synchronizes its internal clocks with the external BuTiS clocks (T_0 and 25 MHz). Finally, the analog RF sine output signal is generated after the time delay caused by internal processing time and cable delays.

The digital processing and the clock synchronization introduce only a time delay. The analog parts of the output stage (e.g. cables and filters) contribute to the overall time delay, but also add a transient behavior before the output signal of the generator reaches a steady state (during beam operation, this transient behavior occurs only at the phase reset of the Group DDS and has decayed before injection of the beam). Both of the time delays defined above are described by the cumulative dead time τ_δ from the start of the resynchronization process to the moment when the RF sine wave signal is available at the output of the DDS module.

As shown in Fig. 4, the measurement for the calibration is triggered by a two-stage trigger condition: First, the rising edge of the DDS trigger output has to occur (condition A). After that, the rising edges of T_0 are counted up to the (user-defined) number N_{ref} (condition B).

At this point one can see that the overall precision is dependent on BuTiS, and it is possible to use one of the clock signals as the reference for the absolute phase calibration. After an introduction of sine wave fit algorithms (Section 4.2), a relationship between the rising edge of the BuTiS T_0 and the phase of the signal under calibration at the beginning of the sine wave cycle will be formulated in Section 4.3.

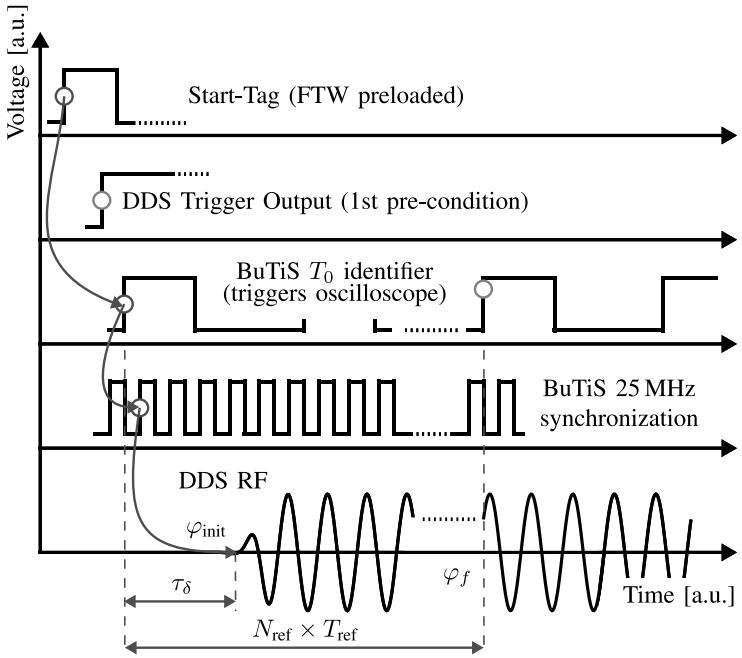

Fig. 4. Resynchronization and trigger sequence.

4.2. Sine wave fit algorithms

Consider a sine wave signal $v(t)$ with a fundamental angular frequency $\omega = 2\pi f$ which may also contain higher harmonics and noise. The measured signal is represented by a sequence of samples y_n taken at (not necessarily equally spaced) time instants t_n with $n \in \{1, \dots, N\}$. The waveform of this signal can be described by the function

$$\begin{aligned} v(t_n) &= C + \sum_{h=1}^{H} V_h \sin(h\omega t_n + \phi_{h,f}) \\ &= C + \sum_{h=1}^{H} \left(A_h \cos(h\omega t_n) + B_h \sin(h\omega t_n) \right), \end{aligned} \tag{1}$$

where C is the offset, V_h and $\phi_{h,f}$ are the amplitude and phase of harmonic h, A_h and B_h are the in-phase and in-quadrature amplitudes of harmonic h, and H is the total number of considered harmonics. Note that, for the considered application, the amplitude of the main harmonic is in general larger than the higher harmonics, i.e. $V_1 \gg V_h$ for $h > 1$. However, the higher harmonics will be included as an additional degree of freedom in order to increase the fit accuracy.

Sine wave fit algorithms allow to estimate the unknown parameters of the sampled sine wave signal that minimize the least square error between the acquired data samples and the signal model given by Eq. (1). In case the frequency ω is known and three parameter types are unknown, the 3PSF algorithm can be used. For unknown frequency, the 4PSF algorithm is needed. In the following, the 3PSF and the 4PSF grid-search algorithms of [32] are extended in a straightforward way to include also the higher harmonics.

Using

$$\mathbf{v} = \begin{pmatrix} v(t_1), & \dots, & v(t_N) \end{pmatrix}^{\mathrm{T}},$$

function (1) can also be written in matrix form as

$$\mathbf{v} = \mathbf{D}(\omega)\mathbf{x}$$

with the $N \times (2H + 1)$ matrix

$$\mathbf{D}(\omega) = \begin{pmatrix} \cos(\omega t_1) & \sin(\omega t_1) & \cos(2\omega t_1) & \sin(2\omega t_1) & \cdots \\ \cos(\omega t_2) & \sin(\omega t_2) & \cos(2\omega t_2) & \sin(2\omega t_2) & \cdots \\ \vdots & \vdots & \vdots & \vdots & \ddots \\ \cos(\omega t_N) & \sin(\omega t_N) & \cos(2\omega t_N) & \sin(2\omega t_N) & \cdots \end{pmatrix} \begin{matrix} \cos(H\omega t_1) & \sin(H\omega t_1) & 1 \\ \cos(H\omega t_2) & \sin(H\omega t_2) & 1 \\ \vdots & \vdots & \vdots \\ \cos(H\omega t_N) & \sin(H\omega t_N) & 1 \end{matrix} \tag{2}$$

and the parameter vector

$$\mathbf{x} = \begin{pmatrix} A_1, & B_1, & A_2, & B_2, & \dots, & A_H, & B_H, & C \end{pmatrix}^{\mathrm{T}}.$$

Combining the measured samples into

$$\mathbf{y} = \begin{pmatrix} y_1, & \dots, & y_N \end{pmatrix}^{\mathrm{T}}$$

and using the least-squares procedure of [32] to minimize $\|\mathbf{y} - \mathbf{v}(\mathbf{x})\|_2$ leads to the estimation

$$\hat{\mathbf{x}} = (\mathbf{D}(\omega)^{\mathrm{T}}\mathbf{D}(\omega))^{-1}\mathbf{D}(\omega)^{\mathrm{T}}\mathbf{y} \tag{3}$$

in case the frequency ω is known (3PSF).

For an unknown frequency, the optimization problem becomes nonlinear in the unknown parameters and the 4PSF has to be employed, for example an iterative procedure based on the initial estimates or by a grid search [28,29]. The present description concentrates on the latter approach allowing to avoid direct implementation of the 4PSF. First, a separate initial frequency estimation is calculated, followed by the 3PSF estimating the remaining unknown parameters. The frequency grid can be determined using a DFT of the sampled signal. A one-dimensional grid search [32] is then employed to obtain the corresponding frequency estimate by

$$\hat{\omega} = \arg\max_{\omega} g(\omega) \tag{4}$$

where

$$g(\omega) = \mathbf{y}^{\mathrm{T}}\mathbf{D}(\omega) \left(\mathbf{D}(\omega)^{\mathrm{T}}\mathbf{D}(\omega) \right)^{-1} \mathbf{D}(\omega)^{\mathrm{T}}\mathbf{y}. \tag{5}$$

This process can be repeated for several iterations in order to improve both the frequency grid resolution and the resulting frequency estimate. Finally, the estimates of the remaining unknown parameters are obtained from Eq. (3) by replacing ω with $\hat{\omega}$.

4.3. Calculation of the phase corrections

Using the model of an acquired sine wave signal given by Eq. (1), the new method works as follows. Consider a sampled signal with a constant frequency f provided by the DDS module that operates at fundamental harmonic. The phase of harmonic h of this signal can be obtained as [43]

$$\phi_{h,f} = \text{atan2}\left(A_h, B_h\right) \tag{6}$$

where A_h and B_h are the parameters estimated by the sine fit algorithms introduced in Section 4.2. Since only the phase of the fundamental component, $\phi_{1,f}$, is relevant for our application, we omit the subscript 1 to simplify the notation.

An illustration of the measurement procedure is given in Fig. 4. At the moment when the oscilloscope is triggered, the phase of the ideal signal, where no phase deviations are present, is

$$\phi_f - \phi_{\text{init}} = 2\pi f \left(N_{\text{ref}} T_{\text{ref}} - \tau_\delta\right). \tag{7}$$

Here, $T_{\text{ref}} = 10\,\mu\text{s}$ is the period of the T_0 reference pulse and N_{ref} is the number of its periods skipped. This skipping is necessary to avoid that the transient part of the signal degrades the measurement accuracy. The measured, non-ideal phase can be expressed as

$$\phi_{\text{meas},f} - \phi_{\text{init}} = 2\pi f \left(N_{\text{ref}} T_{\text{ref}} - \tau_\delta\right) + \phi_{\text{e},f} \tag{8}$$

with the additional phase error $\phi_{\text{e},f}$ at frequency f. In order to eliminate the error, one has to modify ϕ_{init} in such a way that $\phi_{\text{meas},f}$ is equal to ϕ_f:

$$\phi_f - \phi_{\text{init, new}} = 2\pi f \left(N_{\text{ref}} T_{\text{ref}} - \tau_\delta\right) + \phi_{\text{e},f} \tag{9}$$

The difference (7)–(9) yields

$$\phi_{\text{init, new}} - \phi_{\text{init}} = -\phi_{\text{e},f}. \tag{10}$$

Hence, the phase of the DDS module must be adjusted with an additional phase correction $\phi_{\text{init, new}} = -\phi_{\text{corr},f}$ to compensate for the phase error $\phi_{\text{e},f}$. The phase error $\phi_{\text{e},f}$ is obtained from (8) by setting the initial phase of the DDS ϕ_{init} to zero:

$$\phi_{\text{e},f} = \phi_{\text{meas},f} - 2\pi f \left(N_{\text{ref}} T_{\text{ref}} - \tau_\delta\right) \tag{11}$$

Since the phase correction values should be periodic with a period of 2π, the calculated phase error is mapped to the interval $(-\pi, \pi]$:

$$\phi_{\text{corr},f} = \pi - \left[\left(-\phi_{\text{e},f} + \pi\right) \bmod 2\pi\right] \tag{12}$$

A suitable definition of τ_δ allows to accurately determine $\phi_{\text{e},f}$ and to avoid a large phase advance over the calibrated frequencies interval. However, in many cases it is difficult to clearly determine the start of the analog output signal generation due to the present noise. In our application we utilize $\tau_\delta = 1.494\,\mu\text{s}$, which was derived from repetitive oscilloscope measurements of the time interval between the start of the resynchronization process and the generation of the output signal, as illustrated in Fig. 4. We choose $N_{\text{ref}} = 5$ which gives a 50 µs delay to guarantee that the transient behavior is omitted and the generator's output is stable.

4.4. Measurement setup

A schematic diagram of the measurement setup is given in Fig. 5. The calibration sequence is controlled via PC (for the standard operation at FAIR the PC's functionality will be delegated to a controller hardware that can be controlled by the CCS). The PC initializes the calibration procedure via FAIR's front end controller SCU, which sends an FTW corresponding to the frequency under calibration to the dedicated DDS module. The DDS module itself is supplied with the clock signals from the dedicated BuTiS distribution amplifier, allowing to realize the resynchronization principle described in Sections 2.1 and 4.1. The signals are sampled with a digital oscilloscope (DSO) and transferred to the PC which calculates the phase correction. The obtained phase corrections are written into the flash memory of the CEL using a JTAG (Joint Test Action Group) port.

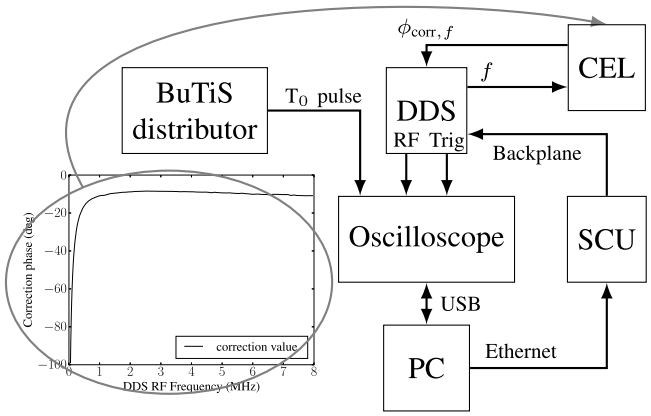

Fig. 5. Measurement setup for the calibration.

4.5. Triggering

The oscilloscope is set to a sequential trigger mode. Dependent on the manufacturer, this trigger type may also be denoted as a qualified or a logic trigger. The rising edge of the DDS trigger output signal arms the oscilloscope. This first condition indicates that the DDS has processed the new frequency tuning word. The second condition and the actual trigger source is the rising slope of one of the following BuTiS T_0 pulses. Since the oscilloscope is not triggered immediately on the first occurrence of the T_0 pulse, the corresponding number of skipped trigger events N_{ref} must be subtracted according to (11).

4.6. Proposed calibration procedure

Although the description of the proposed method is given with respect to our application, it is further applicable to spatially distributed RF systems, which are used to produce phase-synchronous frequency-variable RF signals. From the above analysis, the calibration procedure can be established as follows:

1. define and fix τ_δ and N_{ref} in order to process steady-state waveforms;
2. set ϕ_{init} to zero and select the desired frequency;
3. initiate the trigger sequence consisting of a reference clock pulse train, the digital frequency synthesizer signal under calibration and the corresponding identifier pulse analog to Fig. 4;
4. read out the acquired data and determine $\phi_{\text{meas},f}$ by a fit algorithm;
5. calculate $\phi_{\text{corr},f}$ according to (11) and (12);
6. repeat steps 2–5 for every frequency f in the frequency interval under calibration.

5. Setting of measurement parameters

It can be seen that the DDS RF signals' phase accuracy estimation depends on different measurement parameters and on the performance of the sine fit algorithm [32]. Assuring convergence of the estimated phases and minimizing their deviation allows to increase the precision of the calibration. On the other hand, from a practical standpoint, it is necessary to decrease the computing time needed to analyze each sine wave and hence to decrease the time needed for the whole calibration procedure. Thus a suitable choice of parameters is of importance.

The results presented in the following are based on real DDS signals sampled with a digital oscilloscope (LeCroy Waverunner 64Xi). The analysis has been conducted on a Windows-based 64-bit laptop computer with a 2.6 GHz dual-core CPU and 16 GB of RAM. For the analysis, each of the examined parameters was varied while other

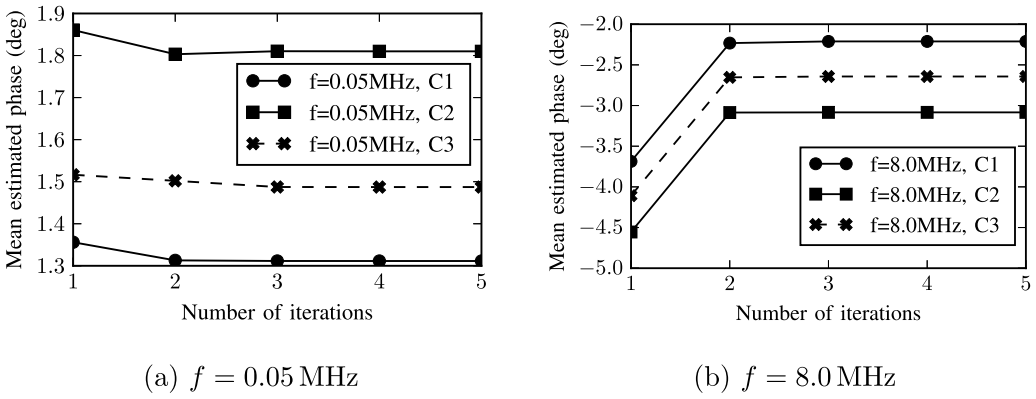

Fig. 6. Dependence of the estimated phase on the number of iterations for frequency grid search.

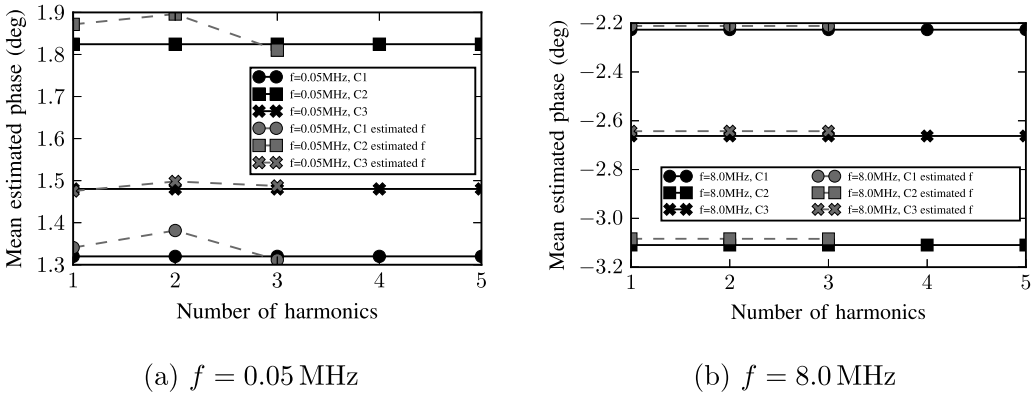

Fig. 7. Dependence of the estimated phase on the number of harmonics, number of iterations for frequency grid search: 3. Black markers refer to the 3PSF result (known frequency), gray markers to the 4PSF (estimated frequency).

parameters remained unchanged. This study focuses on the following set of parameters: the sine fit parameters, the amount of data for the sine fit and the number of measurements for each frequency under calibration. Their detailed description is given in the following sections, where we investigate their impact and define a compromise for our application.

5.1. Sine fit parameters

For the algorithm itself, the following two parameters have to be fixed:

5.1.1. Number of iterations for frequency grid search

If the frequency of the sine wave is estimated, the frequency grid resolution is improved with an increased number of iterations, which allows to achieve a better fit of the sampled data and to improve the phase estimation. However, it also increases the time needed to process the data. The study shows that sufficient convergence of the mean estimated phases is achieved after 3 iterations of the frequency grid search (Fig. 6; here and throughout the whole paper, "C" is used to distinguish between the oscilloscope channels measuring different DDS modules). This value is then used to make a comparison with the sine fit algorithm without frequency estimation.

5.1.2. Number of harmonics included in the fitting function

Fig. 7 shows the dependence of phases estimated by the sine fit algorithm on the number of harmonics used to perform the fit for the case with frequency estimation (4PSF) and with known frequency (3PSF), respectively. One sees that the phase estimated with the known frequency does not change with the number of harmonics used to perform the estimation. Hence it is in principle possible to use only the first harmonic to achieve convergence. On the other hand, the estimated phase of the sine wave improves with the number of harmonics used for the fit when the frequency is estimated. The difference between values estimated by the two approaches (with and without frequency estimation) decreases with the number of harmonics increased, which can be explained by numerical errors due to harmonic distortion [44]. From Fig. 7 one can note that this difference is below $0.1°$, which is far below our accuracy requirements. These results also confirm that the DDS modules steadily realize a FTW with a very good accuracy. The average processing times for one measurement when the 3PSF algorithm is used are 10.8 ms, 19.8 ms, 29 ms, 37.7 ms and 47.4 ms for the number of harmonics from 1 to 5, respectively. The following processing times are obtained for the number of harmonics 1, 2 and 3 when the 4PSF algorithm is used: 1.9 s, 3.3 s and 4.9 s, respectively. Not surprisingly, whenever the frequency is known the 3PSF should be favored over the 4PSF due to its computing time being two orders of magnitude lower with comparable accuracy, which is sufficient to achieve our requirements.

During the development stage of the DDS generators, an FTW sent via the SCU sometimes was not adopted by the DDS from time to time. In order to help detecting these occurrences the unknown frequency model and the corresponding 4PSF has been implemented along with the 3PSF algorithm. In the present state the calibration procedure employs the 3PSF algorithm for the phase estimation and monitors the fit performance calculated as a normalized root-mean-square deviation. If the fit error exceeds a threshold value, then a sine fit with the frequency estimation, i.e. the 4PSF, is performed for diagnostic purposes. This allows achieving a convergence of estimated phase values and minimizing the time needed for the calibration.

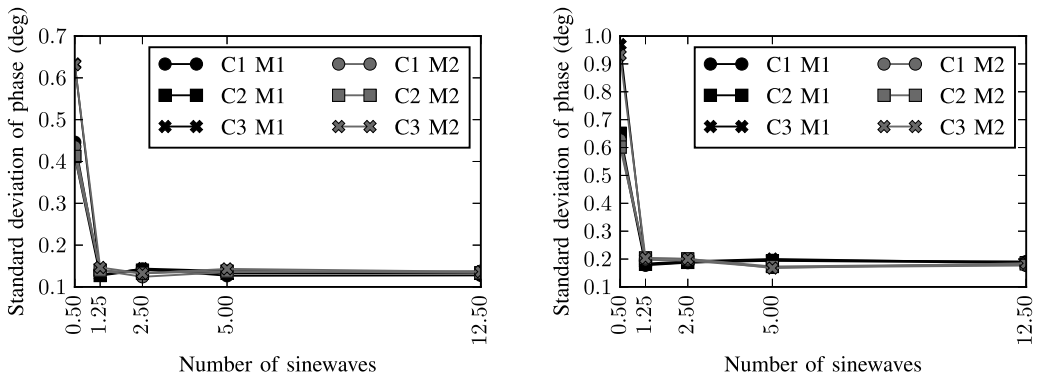

(a) $f = 0.25\,\mathrm{MHz}$ (b) $f = 2.5\,\mathrm{MHz}$

Fig. 8. Dependence of the standard deviations of the estimated phases on the number of sine waves, number of measurements: 500.

5.2. Amount of data for sine fit

For further optimization of parameters the 3PSF is employed with 1 harmonic considered for the fitting function. The amount of data is determined by the following parameters:

5.2.1. Number of sine waves per measurement trace

Fig. 8 shows the standard deviations of estimated phases as functions of the number of sine waves, i.e. number of acquired sine-wave cycles. For both frequencies two measurement series of 500 measurements (hereinafter denoted as M1 and M2) were recorded for each number of sine waves. In this case the standard deviation of the estimated phase is mainly due to the error of the method itself, and the random error is minimized. From Fig. 8 one may note a constant standard deviation of phases if more than one RF period of the sine wave is sampled. This demonstrates that processing data series with non-integer number of sine waves does not introduce any numerical artifacts, which allows one to perform the calibration with an arbitrary frequency step, with no need to maintain a certain integer number of sine waves.

5.2.2. Number of samples per sine wave

In Fig. 9 the results obtained by changing the number of samples per sine wave are shown. The estimation of sine wave parameters improves with an increasing number of samples [30], while the processing time increases. Therefore, the choice of this parameter is determined by the compromise between the desired level of accuracy and the processing time. From Fig. 9 one sees that by increasing the number of samples per sine wave the mean estimated phase is improved, and the level of accuracy sufficient for our application can be achieved with 2000 samples per sine wave. In general, this parameter should be increased if a higher level of accuracy is desired.

5.2.3. Number of measurements for frequency under calibration

From a practical point of view it is not necessary to acquire and process long data series during the routine calibration. In Figs. 10(a) and 10(b) the dependencies of the standard deviations of estimated phases on the number of sine waves for 10 and 30 measurements, respectively, are shown. It can be observed that by increasing the number of measurements, the random error of the measurement is reduced, and the standard deviations of phases converge to a nonzero value, which is $\Delta\varphi \approx \pm 0.15°$ for the frequency $f = 0.25\,\mathrm{MHz}$.

The remaining error and therefore the uncertainty of the phase measurement includes a jitter of the reference signal and oscilloscope timebase errors. In addition, the phase $\phi_{\mathrm{meas},f}$ returned by the 3PSF algorithm is subject to an estimation uncertainty defined by the signal-to-noise-ratio and the finite number of samples [30].

Table 1
Obtained recommended measurement parameters.

Parameter	Known frequency (3PSF)	Unknown frequency (4PSF)
Number of harmonics	1	3
Number of iterations	n.a.[a]	3
Number of sine waves	2–10	
Number of samples	2000	
Number of measurements	30	

[a] Frequency grid search is not performed if the frequency is known.

The summary of the obtained measurement parameters that are regarded as recommended parameters (based on the detailed analysis) for our application is given in Table 1. The recommended amount of data used for the sine fit is maintained by a lookup table. For this purpose the oscilloscope's time per division and the number of samples settings for every frequency in the frequency range under calibration are adjusted automatically.

6. Application: SIS18 group DDS calibration

The presented method with the obtained recommended parameters was applied for the calibration of the Group DDS modules in the supply area of the SIS18 synchrotron. In the SIS18 supply area the output signals of the DDS modules, in contrast to the laboratory environment, are not terminated at the oscilloscope input. Instead they are delivered to the corresponding systems by means of Distribution Amplifiers and the Switch Matrix (Fig. 1). In this arrangement the influence of the uppermost Distribution Amplifier is also compensated with the calibration. For the calibration a frequency interval from 50 kHz to 8.1 MHz was covered with 92 non-equidistant frequency points. The computational time for the complete calibration procedure for one module was around 12 min on a Windows-based 64-bit 2.5 GHz dual-core system with 8 GB of RAM. A piecewise polynomial interpolation was used to obtain smooth calibration curves from the measured points.

The obtained phase calibration curves for Group DDS modules A–D are shown in Fig. 11(a). Please note that the DDS module D (which corresponds to a different hardware revision) produces an RF signal with the reversed polarity, therefore its phase correction curve is flipped by 180° with respect to the correction curves of other modules. A "wobbling" pattern in the measured calibration curves can be explained by reflections in the topology. The distance between adjacent maxima or minima of these waves in the calibration curves is approximately 850 kHz. The Andrew FSJ1-50A coaxial cables between the tee adapters connected to the oscilloscope and the inputs of the second

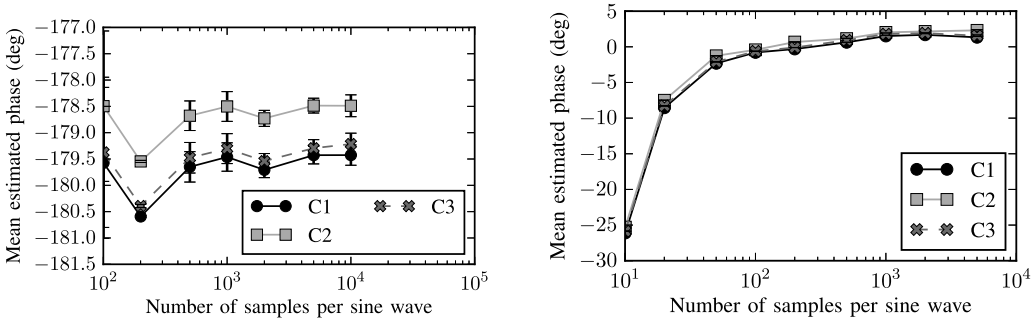

Fig. 9. Dependence of the estimated phase on the number of samples per sine wave, frequency $f = 0.05$ MHz.

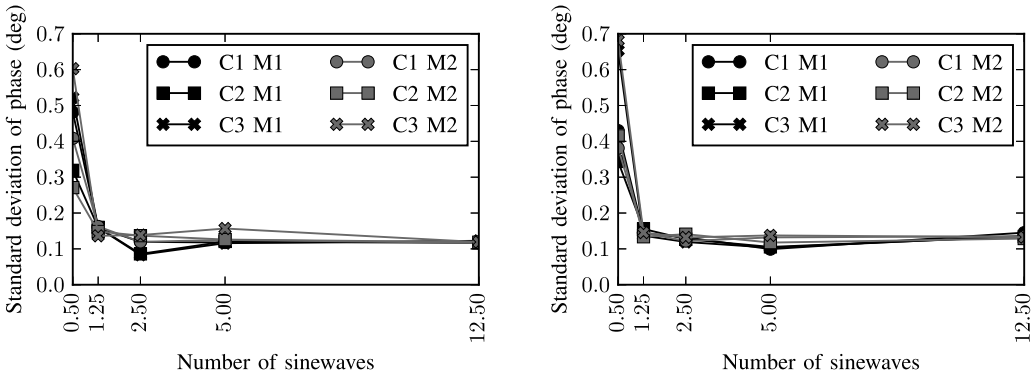

Fig. 10. Dependence of the standard deviations of estimated phases on the number of sine waves, frequency $f = 0.25$ MHz.

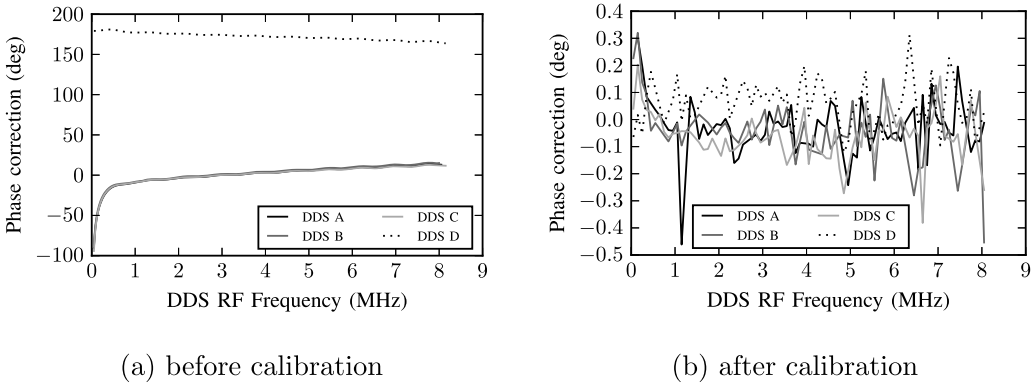

Fig. 11. Example for calibration curves before 11(a) and after calibration 11(b). Please note the different scales in the diagrams on the left and on the right.

distribution amplifier have an electrical length of 585 ns. Assuming a half-wavelength resonance in this transmission line one obtains

$$\Delta f = \frac{1}{2}\frac{1}{t_{\text{delay}}} = 854.7\,\text{kHz} \tag{13}$$

which is close to the calculated frequency interval. Thus, the wobbling pattern can be explained by the half-wavelength resonance in the Andrew FSJ1-50A cables. These results show that the calibration result depends not only on the signal path before the calibration point, but it is also affected by the components in the signal path after the calibration point, i.e. the subsequent coaxial cable FSJ1-50A and the second distribution amplifier. The peak-to-peak amplitude of the waves in the calibration curve is $\Delta\phi_{\text{ref}} \leq 6°$. These effects should be analyzed in detail, even if their effect is rather small.

After the calibration data for each DDS module were loaded into the CEL module, the procedure was repeated in order to verify the calibration. The remaining phase response of the Group DDS modules including the distribution amplifier is within the margins of the phase accuracy requirements (Fig. 11(b)). This demonstrates a successful calibration of the reference RF signals.

The calibrated Group DDS modules were used during the SIS18 beam time in 2018. On July 6$^{\text{th}}$, 2018, the Group DDS signals were measured during beam operation to investigate the phase accuracy under dynamic conditions. The Group DDS modules were configured as follows: $h = 1$ (DDS A), $h = 5$ (DDS B), $h = 1$ (DDS C), and $h = 1$ (DDS D). In order not to disturb beam operation, the measurements were done in a parasitic way by measuring segments

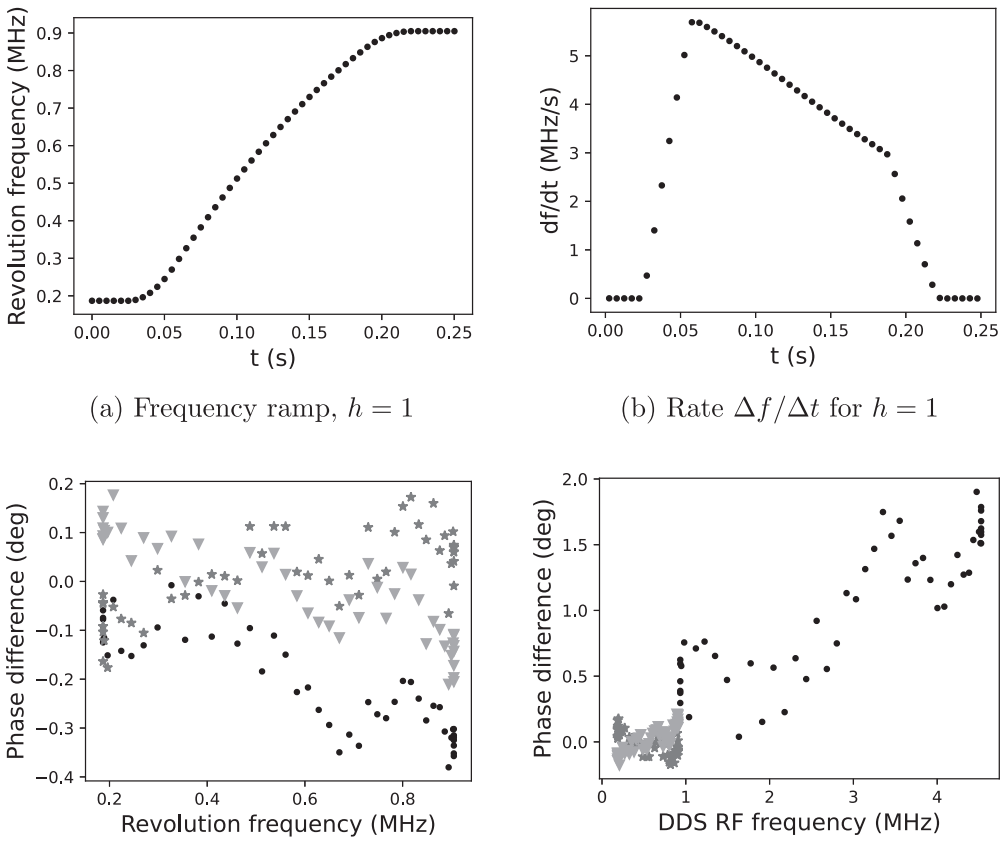

(a) Frequency ramp, $h = 1$

(b) Rate $\Delta f/\Delta t$ for $h = 1$

(c) DDS A compared to B (•), C (⋆), and D (▽)

(d) DDS B (•), C (⋆), and D (▽) compared to A

Fig. 12. Measurement results of a SIS18 cycle during beam operation on July, 6th, 2018.

of 10 µs length every 5 ms. For each segment, a 4PSF was performed for each DDS signal (since the frequency within each segment was not exactly known). The revolution frequency ramp obtained by the fit of DDS A ($h = 1$) is shown in Fig. 12(a): The frequency started at 187 kHz at flat-bottom and increased to 4.525 MHz at flat-top in about 200 ms. The ramp rate calculated from the revolution frequency ramp is shown in Fig. 12(b); its maximum value was roughly 5.7 MHz/s. This corresponds to a frequency change of 57 Hz within 10 µs. Thus, within each measured segment, the frequency of the DDS signals changed by less than 10 ppm, and the phase error due to the frequency change was less than $360° \cdot \Delta f \cdot \Delta t \approx 360° \cdot 57\,\text{Hz} \cdot 10\,\mu s \approx 0.21°$.

The comparison of the phase results is shown in Figs. 12(c) and 12(d). Depending on which signal is defined as reference, the result is different: In Fig. 12(c), the phase of DDS A is compared to the three other DDS modules, whereas the situation is reversed in Fig. 12(d). For the DDS modules C and D, the phase results in Fig. 12(d) differ only by a negative sign compared to Fig. 12(d), since they were also configured with harmonic number $h = 1$. For module B ($h = 5$), the factor is -5 for the phase and 5 for the frequency axis. In general, this reflects the fact that the obtained phase error between two signals with different harmonic numbers is of course largest if the phase $\Delta\varphi = 2\pi f_{\text{RF}}\Delta t$ is measured using the frequency $f_{\text{RF}} = hf_{\text{R}}$ with the larger harmonic number h (here $h = 5$). However, the obtained maximum phase errors are all well below ±3°, which demonstrates the feasibility of the calibration method also under dynamic conditions.

7. Multi-harmonic operation

A successful Group DDS calibration alone is not sufficient to enable multi-harmonic operation with high phase accuracy. In addition to the calibration of the Group DDS, further steps are needed. The target values for the cavity gap voltage amplitude and phase can be calibrated by a cavity calibration procedure, measuring the gap voltage in the RF supply area for different frequencies and amplitudes [45]. This procedure leads to phase and amplitude calibration curves that are also realized by CEL modules and that compensate inaccuracies of the local LLRF control loops. However, there still remain inaccuracies that cannot be eliminated by such measurements. In particular, capacitive gap voltage dividers are needed to obtain the LLRF gap signals (cf. Fig. 1, accelerator tunnel). These gap voltage dividers are situated close to the ceramic gap of the cavity and realize a signal amplitude reduction by typically three orders of magnitude. The gap voltage monitoring, which is realized by a transmission of the gap voltage divider signals into the supply area, must be as accurate as possible [46]. Since the gap voltage dividers cannot be readily reproduced in the signal path of the Group DDS, any frequency-dependent phase response of these dividers that differs from the linear phase response of a pure delay (the delay part can be compensated by cables near the Group DDS) will thus lead to phase errors that cannot be directly measured in the RF supply area. Therefore, dedicated machine experiments with beam are indispensable as a last step to validate the overall phase accuracy by analyzing the beam behavior. Different scenarios have been used at SIS18, e.g. de-bunching [45], dual-harmonic [47], and merging and compression [48]. In SIS18, the errors due to the gap voltage dividers are typically in the order of a few degrees over the complete frequency range. In case these inaccuracies are not acceptable, the cavity calibration procedure could in principle use the measured transfer function of the gap voltage dividers to calculate a correction of the measured gap voltage and obtain more accurate calibration curves. However, this

adds an additional level of complexity to the gap signal measurement that may be error-prone and is therefore currently not planned.

8. Conclusion and outlook

In this paper, an application of 3PSF and 4PSF algorithms for phase calibration of frequency-variable RF signals is shown. In the proposed approach a DSO is used to sample analog signals from a digital frequency synthesizer and its clock pulse train. It is demonstrated how to obtain a phase correction at each frequency with respect to the reference pulse train using the information on the precise activation of digital data. A set of parameters influencing the accuracy of the obtained phases is discussed and recommended parameters for our application are derived. The accuracy achieved with respect to the Group DDS modules with $h = 1$ is better than $\pm 0.5°$ for the whole frequency range of interest. The method is applied for the calibration of the SIS18 Group DDS modules. Experimental data demonstrates that the proposed approach meets the phase accuracy requirements of the FAIR synchrotrons' LLRF systems for multi-harmonic operation.

Applications of sine wave parameter estimation algorithms for phase measurement at a given frequency and phase difference estimations were shown in [35,49] and their performance was compared in [27]. To the best of our knowledge, this is the first time that the phase calibration based on the sine fitting algorithms is applied to generate frequency-variable signals in the given frequency range. Further research may focus on application and subsequent comparison of other sine wave phase estimation methods (such as I/Q demodulation) in order to improve the computing time and accuracy of the proposed method.

Declaration of competing interest

The authors declare that they have no known competing financial interests or personal relationships that could have appeared to influence the work reported in this paper.

Data availability

Data will be made available on request.

Acknowledgments

The authors would like to thank our colleagues from the Ring RF department at the GSI Helmholtzzentrum für Schwerionenforschung, especially S. Schäfer, B. Zipfel and P. Hülsmann as well as D. Domont-Yankulova for their proposals and fruitful discussions. Furthermore, the authors thank the reviewers for their valuable comments.

References

[1] M. Vretenar, Radio frequency for particle accelerators: Evolution and anatomy of a technology, in: R. Bailey (Ed.), Proc. CAS–CERN Accelerator School: RF for Accelerators, Ebeltoft, Denmark, 2010, pp. 1–14.
[2] A. Schnase, Cavities with a swing, in: J. Miles (Ed.), CAS–CERN Accelerator School: Radio Frequency Engineering, Seeheim, Germany, 2000, pp. 236–272.
[3] H. Klingbeil, U. Laier, D. Lens, Theoretical Foundations of Synchrotron and Storage Ring RF Systems, Springer International Publishing, Cham, Switzerland, 2015, http://dx.doi.org/10.1007/978-3-319-07188-6.
[4] H. Gutbrod, et al., FAIR–Baseline, Technical Report, GSI, 2006.
[5] P. Spiller, et al., Status of the FAIR project, in: Proc. 9th Int. Part. Accel. Conf., Vancouver, BC, Canada, 2018, pp. 63–68, http://dx.doi.org/10.18429/jacow-ipac2018-mozgbf2.
[6] P. Spiller, et al., The FAIR Heavy Ion Synchrotron SIS100, J. Instrum. 15 (2020) T12013, http://dx.doi.org/10.1088/1748-0221/15/12/T12013.
[7] H. Wiedemann, Particle Accelerator Physics, Springer, Berlin, Heidelberg, 2007, http://dx.doi.org/10.1007/978-3-540-49045-6.
[8] T. Schilcher, RF applications in digital signal processing, in: D. Brandt (Ed.), Proc. CAS–CERN Accelerator School: Digital Signal Processing, Sigtuna, Sweden, 2007, pp. 249–283.
[9] H. Klingbeil, A fast DSP-based phase-detector for closed-loop RF control in synchrotrons, IEEE Trans. Instrum. Meas. 54 (3) (2005) 1209–1213, http://dx.doi.org/10.1109/TIM.2005.847138.
[10] K. Will, A. Omar, Phase measurement of RF devices using phase-shifting interferometry, IEEE Trans. Microw. Theory Tech. 56 (11) (2008) 2642–2647, http://dx.doi.org/10.1109/TMTT.2008.2005892.
[11] Z. Wang, L. Mao, R. Liu, High-accuracy amplitude and phase measurements for low-level RF systems, IEEE Trans. Instrum. Meas. 61 (4) (2012) 912–921, http://dx.doi.org/10.1109/TIM.2011.2179334.
[12] S. Tang, et al., A beam phase and energy measurement instrument based on direct RF signal IQ undersampling technique, IEEE Trans. Instrum. Meas. 61 (11) (2012) 2870–2878, http://dx.doi.org/10.1109/TIM.2012.2200398.
[13] S. Jablonski, K. Czuba, F. Ludwig, H. Schlarb, 2π Low drift phase detector for high-precision measurements, IEEE Trans. Nucl. Sci. 62 (3) 1142–1148, http://dx.doi.org/10.1109/TNS.2015.2425733.
[14] H. Klingbeil, et al., New digital low-level RF system for heavy-ion synchrotrons, Phys. Rev. ST Accel. Beams 14 (10) (2011) 102802, http://dx.doi.org/10.1103/physrevstab.14.102802.
[15] A. Andreev, H. Klingbeil, D. Lens, Phase calibration of synchrotron RF signals, in: Proc. 8th Int. Part. Accel. Conf., Copenhagen, Denmark, 2017, pp. 3945–3947.
[16] M. Thieme, W. Panschow, S. Rauch, SCU system goes productive, in: GSI Scientific Report, GSI, Darmstadt, Germany, 2013, p. 377.
[17] F. Tamura, et al., Development of next-generation LLRF control system for J-PARC Rapid Cycling Synchrotron, IEEE Trans. Nucl. Sci. 66 (7) (2019) 1242–1248, http://dx.doi.org/10.1109/TNS.2019.2899358.
[18] F. Tamura, et al., Commissioning of the next-generation LLRF control system for the Rapid Cycling Synchrotron of the Japan Proton Accelerator Research Complex, Nucl. Instrum. Methods Phys. Res. A 999 (2021) 165211, http://dx.doi.org/10.1016/j.nima.2021.165211.
[19] H. Damerau, D. Perrelet, Upgrade of the beam-synchronous RF source system in the CERN PS, in: Proc. Low Level Radio Frequency Workshop, Barcelona, Spain, 2017.
[20] M.E. Angoletta, Digital low level RF, in: Proc. 10th Eur. Part. Accel. Conf., Edinburgh, U.K., 2006, pp. 1847—1852.
[21] M.E. Angoletta, et al., The new LEIR digital Low-Level RF system, in: Proc. 8th Int. Part. Accel. Conf., Copenhagen, Denmark, 2017, pp. 4062–4065.
[22] B. Zipfel, P. Moritz, Recent progress on the technical realization of the bunch phase timing system BuTiS, in: Proc. 2nd Int. Part. Accel. Conf., San Sebastián, Spain, 2011, pp. 418–420.
[23] M. Bousonville, J. Rausch, Universal picosecond timing system for the Facility for Antiproton and Ion Research, Phys. Rev. ST Accel. Beams 12 (4) (2009) 042801, http://dx.doi.org/10.1103/PhysRevSTAB.12.042801.
[24] S. Schäfer, H. Klingbeil, U. Hartel, A. Klaus, B. Zipfel, Use of FPGA-based configurable electronics to calibrate cavities, in: Proc. 4th Int. Part. Accel. Conf., Shanghai, China, 2013, pp. 3152–3154.
[25] B. Zipfel, et al., Generation of RF frequency and phase references on the FAIR site, in: Proc. 5th Int. Part. Accel. Conf., Dresden, Germany, 2014, pp. 3131–3133.
[26] J.G. Webster, H. Eren (Eds.), Measurement, Instrumentation, and Sensors Handbook: Electromagnetic, Optical, Radiation, Chemical, and Biomedical Measurement, CRC Press, Boca Raton, FL, 2014.
[27] M. Sedlacek, M. Krumpholc, Digital measurement of phase difference–A comparative study of DSP algorithms, Metrol. Meas. Syst. XII (4) (2005) 427–448.
[28] IEEE Standard for Digitizing Waveform Recorders, IEEE, 2008.
[29] IEEE Standard for Terminology and Test Methods for Analog-to-Digital Converters, IEEE, 2011.
[30] T. Andersson, P. Händel, IEEE Standard 1057, Cramér–Rao bound and the parsimony principle, IEEE Trans. Instrum. Meas. 55 (1) (2006) 44–53, http://dx.doi.org/10.1109/TIM.2005.861497.
[31] S. Negusse, P. Händel, P. Zetterberg, IEEE-STD-1057 three parameter sine wave fit for SNR estimation: Performance analysis and alternative estimators, IEEE Trans. Instrum. Meas. 63 (6) (2014) 1514–1523, http://dx.doi.org/10.1109/TIM.2013.2293226.
[32] P. Händel, Properties of the IEEE-STD-1057 four-parameter sine wave fit algorithm, IEEE Trans. Instrum. Meas. 49 (6) (2000) 1189–1193, http://dx.doi.org/10.1109/19.893254.
[33] T.Z. Bilau, T. Megyeri, A. Sárhegyi, J. Márkus, I. Kollár, Four-parameter fitting of sine wave testing result: Iteration and convergence, Comput. Stand. Interfaces 26 (1) (2004) 51–56, http://dx.doi.org/10.1016/S0920-5489(03)00062-X.
[34] M.F. da Silva, P.M. Ramos, A.C. Serra, A new four parameter sine fitting technique, Measurement 35 (2) (2004) 131–137, http://dx.doi.org/10.1016/j.measurement.2003.08.006.
[35] N.M. Vučijak, L.V. Saranovac, A simple algorithm for the estimation of phase difference between two sinusoidal voltages, IEEE Trans. Instrum. Meas. 59 (12) (2010) 3152–3158, http://dx.doi.org/10.1109/TIM.2010.2047155.
[36] D. Belega, D. Petri, D. Dallet, Noise power estimation by the three-parameter and four-parameter sine-fit algorithms, IEEE Trans. Instrum. Meas. 61 (12) (2012) 3234–3240, http://dx.doi.org/10.1109/TIM.2012.2205511.
[37] D. Belega, D. Petri, D. Dallet, Amplitude and phase estimation of real-valued sine wave via frequency-domain linear least-squares algorithms, IEEE Trans. Instrum. Meas. 67 (5) (2018) 1065–1077, http://dx.doi.org/10.1109/TIM.2017.2785098.

[38] D. Belega, D. Dallet, D. Petri, Performance comparison of the three-parameter and the four-parameter sine-fit algorithms, in: Proc. IEEE Instrum. Meas. Technol. Conf, Hangzhou, China, 2011, pp. 340–343, http://dx.doi.org/10.1109/IMTC.2011.5944010.

[39] J. Augustyn, M. Kampik, Improved sine-fitting algorithms for measurements of complex ratio of AC voltages by asynchronous sequential sampling, IEEE Trans. Instrum. Meas. 68 (6) (2019) http://dx.doi.org/10.1109/TIM.2018.2875901.

[40] M. Bertocco, C. Narduzzi, Sine-fit versus discrete Fourier transform-based algorithms in SNR testing of waveform digitizers, IEEE Trans. Instrum. Meas. 46 (2) (1997) 445–448, http://dx.doi.org/10.1109/19.571881.

[41] R. Lapuh, Estimating the fundamental component of harmonically distorted signals from noncoherently sampled data, IEEE Trans. Instrum. Meas. 64 (6) (2015) 1419–1424, http://dx.doi.org/10.1109/TIM.2015.2401211.

[42] R. Lapuh, et al., Uncertainty of the signal parameter estimation from sampled data, in: Proc. Conf. Precis. Electromagn. Meas. Dig., Ottawa, ON, Canada, 2016, pp. 1–2.

[43] IEEE Standard for Floating-Point Arithmetic, IEEE, 2008.

[44] J.P. Deyst, T.M. Sounders, O.M. Solomon, Bounds on leasts-quares four-parameter sine-fit errors due to harmonic distortion and noise, IEEE Trans. Instrum. Meas. 44 (3) (1995) 637—642.

[45] U. Hartel, et al., Precise verification of phase and amplitude calibration by means of a debunching experiment in SIS18, in: Proc. 4th Int. Part. Accel. Conf., Shanghai, China, 2013, pp. 3155–3157.

[46] H. Okita, et al., Improvement of longitudinal beam tracking simulation considering the frequency response of the cavity gap voltage monitor, Nucl. Instrum. Methods Phys. Res. A 1041 (2022) 167361, http://dx.doi.org/10.1016/j.nima.2022.167361.

[47] K.-P. Ningel, et al., Dual harmonic operation at SIS18, in: Proc. 1st Int. Part. Accel. Conf., Kyoto, Japan, 2010, pp. 1410–1412.

[48] D. Lens, et al., Bunch merging and compression: recent progress with RF and LLRF systems for FAIR, in: Proc. 15th Int. Conf. on Heavy Ion Acc. Technology, Darmstadt, Germany, 2022, pp. 67–71.

[49] P.M. Ramos, A.C. Serra, A new sine-fitting algorithm for accurate amplitude and phase measurements in two channel acquisition systems, Measurement 41 (2) (2008) 135–143.